Parametric model to estimate clear-sky longwave irradiance at the surface on the basis of vertical distribution of humidity and temperature

Jean-Charles Dupont, Martial Haeffelin, Philippe Drobinski, T. Besnard

Parametric model to estimate clear-sky longwave irradiance at the surface on the basis of vertical distribution of humidity and temperature

Jean-Charles Dupont,[1,2] Martial Haeffelin,[3] Philippe Drobinski,[4] and Thierry Besnard[5]

Received 5 June 2007; revised 24 September 2007; accepted 16 November 2007; published 8 April 2008.

[1] The surface downwelling longwave irradiance in clear-sky situations is an important component of the global radiation balance. It can be measured directly using ground-based pyrgeometers or computed using a radiative transfer code given precise information on atmospheric composition (water vapor, ozone, and aerosols) and temperature. Discrepancies between instantaneous observed and simulated values of the clear-sky longwave irradiance are typically at the 3–10 W m^{-2} level (root-mean-square error). The discrepancies depend both on pyrgeometer and atmospheric composition uncertainties. Over the past century, many authors have worked on deriving control parameters to simulate the clear-sky longwave irradiance using simple parameterizations. The most common control parameters found in the literature are screen-level temperature, screen-level water vapor density, and column integrated precipitable water. We show that reference parameterizations are able to simulate the clear-sky longwave irradiance with an uncertainty of about 10 W m^{-2}. Uncertainties are greater during nighttime than daytime periods. We propose a new parameterization that uses the standard input parameters and their diurnal variations to account for important effects of their vertical distribution on the simulation of clear-sky longwave irradiance. The new parameterization allows us to reduce uncertainties in clear-sky surface downwelling longwave irradiance simulations to better than 5 W m^{-2} for both daytime and nighttime situations.

Citation: Dupont, J.-C., M. Haeffelin, P. Drobinski, and T. Besnard (2008), Parametric model to estimate clear-sky longwave irradiance at the surface on the basis of vertical distribution of humidity and temperature, *J. Geophys. Res.*, *113*, D07203, doi:10.1029/2007JD009046.

1. Introduction

[2] The downwelling longwave irradiance incident upon the surface of the Earth is a particularly complex term of the global radiation budget. The amplitude of its diurnal cycle, typically less than 100 W m^{-2}, is small compared to that of the solar irradiance. Its variability is dominated by the density of water present along the atmospheric column in the form of vapor, liquid and ice phase. Water vapor molecules present a complex absorption spectrum, with a few strong absorption lines and a continuum of absorption in the infrared atmospheric window that depends on the water vapor density. Liquid or ice water layers radiate at their own radiative temperature. Variations at the diurnal scale in atmospheric column water vapor may induce changes in instantaneous longwave irradiances ranging from 1–2 W m^{-2} to 10–20 W m^{-2}. Persisting effects at the 1–2 W m^{-2} level will lead to significant impacts on the monthly and yearly radiation balance of the same magnitude. The effect of water vapor alone must be accurately quantified in order to study the effect of clouds on the longwave irradiance that typically ranges from a few W m^{-2} to greater than 50 W m^{-2} [*Chen et al.*, 2000; *Shupe and Intrieri*, 2003; *Dong et al.*, 2005]. Cloud effects remain a largely unresolved issue as the sign of cloud feedback to a CO_2 doubling scenario is still not clearly established [*Cess et al.*, 1990; *Watson and the Core Writing Team*, 2001; *Bony et al.*, 2004; *Bernstein and the Core Writing Team*, 2007].

[3] In order to quantify the effect of clouds on the longwave irradiance measured at the surface, one must first establish a reference irradiance defined as the irradiance that one would measure if the cloud was not present. This exercise has been carried out for almost one century, starting with the work of *Ångström* [1918] who developed an empirical relationship between clear-sky emissivity and water vapor pressure at the surface, considering that the clear atmosphere radiates toward the ground like a grey body at a screen-level temperature. Since this work, additional optimized models were developed, to better relate the

[1] Institut Pierre Simon Laplace, Laboratoire de Météorologie Dynamique, Ecole Polytechnique, Palaiseau, France.
[2] Also at ATMOS Sarl, Saint Saturnin, France.
[3] Institut Pierre Simon Laplace, Ecole Polytechnique, Palaiseau, France.
[4] Institut Pierre Simon Laplace, Service d'Aéronomie, Université Pierre et Marie Curie, Paris, France.
[5] ATMOS Sarl, Saint Saturnin, France.

0148-0227/08/2007JD009046

clear-sky atmospheric emissivity with observed surface temperature and water vapor density and compute the instantaneous longwave irradiance with greater accuracy [*Brunt*, 1932; *Swinbank*, 1963; *Idso and Jackson*, 1969; *Brutsaert*, 1975; *Ohmura*, 1981]. Several comparisons and reviews have been carried out and show that the column integrated water vapor density (IWV) is a key variable to estimate the clear-sky atmospheric emissivity [e.g., *Prata*, 1996; *Niemelä et al.*, 2001]. In recent studies, the authors emphasize that such parameterizations perform best after local calibration [*Duarte et al.*, 2006], or if sinusoidal parameterizations are used to adjust for seasonal and diurnal cycles [*Dürr and Philipona*, 2004]. Finally, *Ruckstuhl et al.* [2007] show that the monthly mean downwelling longwave irradiance can be effectively modeled from either specific humidity or IWV.

[4] The clear-sky downwelling longwave irradiance at the surface can also be estimated using radiative transfer model such as SBDART [*Ricchiazzi et al.*, 1998], MODTRAN [*Snell et al.*, 1995], LOWTRAN [*Kneizys et al.*, 1988] by taking into account actual emission and absorption phenomena in the atmosphere. To be accurate and to represent actual conditions, radiative transfer calculation require realistic input data (i.e., temperature and humidity profile, aerosol properties) at each time step. Such data is of course not as readily available as screen-level data. Hence, all the work devoted to develop and improve empirical parameterizations. It is worthwhile to mention that what ever the method (radiative transfer or parameterization), the irradiances that one would measure in the absence of clouds are estimated keeping all other atmospheric parameters constant. Hence these studies consider that the removal of the cloud has no instantaneous effect on the atmosphere thermodynamics.

[5] Currently available state-of-the-art parameterizations can simulate the downwelling clear-sky longwave irradiance with a root-mean-squared uncertainty better than 10 W m^{-2} [*Niemelä et al.*, 2001]. To reduce this uncertainty in order to study cloud effects on a few watt per square meter range, the clear-sky estimations must yet be improved. The goal of this present work is to assess the performance of two well-known models, namely those of *Brutsaert* [1975] and *Prata* [1996], hereinafter referred to as B75 and P96, understand their limitations, and model their residual errors using new control parameters. In section 2, we describe observation data set and parametric models. In section 3, we evaluate performances of these simple models (best local parameters) and we define a new control parameter that considers the impact of vertical profile of water vapor density to improve performances. Next, we relate the residual errors to the vertical profile of temperature. In section 4 we compare simulations to measurements performed at the SIRTA Observatory (Palaiseau, France).

2. Observations and Clear-Sky Model Descriptions

2.1. Observation Data Set

[6] To study the relationship between longwave irradiance at the surface and the state of the atmosphere (temperature and humidity) in clear-sky situations we need the following observations: (1) high-quality longwave irradiance measurements, (2) screen-level temperature and water vapor pressure, (3) column-integrated water vapor density, (4) vertical profiles of temperature and humidity, and finally (5) unambiguous identification of cloud-free situations. We choose to use measurements from the SIRTA Observatory [*Haeffelin et al.*, 2005], a midlatitude (48.7°N, 2.2°E) cloud and aerosol research observatory that gathers active and passive remote sensing instruments since 2002. The site is located in a semiurban area, 25 km south of Paris.

[7] Table 1 summarizes the instruments available at the SIRTA observatory that are used for this study. SIRTA is a Baseline Surface Radiation Network site (BSRN [*Ohmura et al.*, 1998]). Routine radiation measurements are performed using a CH1 pyrheliometer, a shaded CM22 pyranometer for the solar components and a shaded CG4 pyrgeometer for the longwave component. Integrated water vapor (IWV) measurements are provided by the Drakkar vertically pointing dual-channel microwave radiometer. Drakkar participated in a microwave radiometer intercomparison carried out in the CLIWANET project [*Van Meijgaard and Crewell*, 2005] and was successfully used during the CLOUDNET project [*Illingworth et al.*, 2007]. During cloud-free situations, IWV are also obtained by an AERONET Sun photometer (CIMEL 318-CE; 440, 670, 870, 940 and 1020 nm). A GPS (Global Positioning System) receiver was installed in 2006 to complement IWV retrievals [e.g., *Bock and Doerflinger*, 2001].

[8] Temperature, pressure, relative humidity and wind profiles are obtained from RS90 radiosonde measurements performed by Météo-France from Trappes (15 km northwest of SIRTA) at 0000 and 1200 UT as part of their operational network. IWV is also computed by integrating vertical profile of humidity and temperature. A water Vapor Intercomparison Campaign (VAPIC) was carried out at SIRTA in 2004 to assess the uncertainty in current ground-based and satellite water vapor sensors. Intercomparison of collocated microwave radiometer, GPS, Sun photometer and RS90 radiosonde measurements revealed that IWV retrievals were consistent to the 1 kg m^{-2} level. Atmospheric column measurements are complemented by screen-level measurements of wind speed and direction, temperature, pressure, humidity and precipitations. SIRTA operates a dual-channel backscatter depolarization lidar on a routine basis to document the vertical distributions of particles (clouds and aerosols) from 500 m to about 15 km above ground [*Haeffelin et al.*, 2005]. The backscatter lidar is used to identify the presence of liquid or ice water in the atmospheric column.

2.2. Clear-Sky Period Identification

[9] In this study, the term ''clear-sky'' is defined as a sky without any liquid water or ice cloud (high or low altitude, high or low cloud fraction). Clear-sky periods during daytime are selected by an automated method [*Long and Ackerman*, 2000] based on surface measurements of downwelling total, diffuse and direct shortwave radiation with a 1-min sampling period. This method is sensitive to clouds in the entire hemispherical field of view of the pyranometer. However, the impact of high-altitude optically thin clouds (cirrus clouds) on downwelling shortwave radiation can be difficult to detect using a threshold algorithm. We identify the presence of cirrus clouds with the vertically pointing lidar data [*Morille et al.*, 2007] and

Table 1. Instruments Available at the SIRTA Observatory and Periods of Measurements[a]

Instruments	Measurements	Periods of Measurements
CM22 shadow pyranometer	diffuse SW flux	since December 2002
CG4 pyrgeometer	LW flux	since December 2002
CH1 pyrheliometer	direct SW flux	since December 2002
CM22 pyranometer	global SW flux	since October 2005
Surface weather station	T_a, RH, P, PR, WS and WD	since April 2005
Drakkar microwave radiometer	IWV	between 2002 and 2005
GPS	IWV	since March 2006
Sun photometer	IWV	since July 1999
Radiosondings	profiles of T, RH, P, WS and WD	since April 1999
Backscatter lidar	detection of clouds and aerosols	since September 2002

[a]SW, shortwave; LW, longwave; T_a, temperature; RH, relative humidity; P, pressure; PR, precipitation rate; WS, wind speed; WD, wind direction.

remove these situations from the clear-sky data set. Using the combined irradiance-lidar algorithm, we detect 16 clear-sky days with cloud free periods longer than 6 h between May 2004 and October 2005 (5223 2-min periods). We consider long clear-sky periods to obtain wide diurnal variations of atmospheric parameters (temperature, water pressure, integrated water vapor). These days are equitably distributed throughout the calendar year (1 or 2 d per month). For nighttime periods, we use an algorithm based on longwave irradiance to detect periods without clouds [*Dürr and Philipona*, 2004]. Moreover, we constrain this detection with the backscatter lidar and with variations of the liquid water path (measured with the Drakkar microwave radiometer) that must be zero during clear-sky conditions. We detect 16 cloud free nighttime periods lasting more than 4 h (average of 5 h per night) that represent 4877 1-min periods.

2.3. Clear-Sky Model Description

[10] Considering that the atmosphere is a grey body, the clear-sky downwelling longwave irradiance ($LW_{CS\downarrow}$) can be estimated by the Stephan-Boltzmann law [*Ångström*, 1918; *Brunt*, 1932; *Swinbank*, 1963]:

$$LW_{CS\downarrow} = \varepsilon \times \sigma \times T_a^4 \tag{1}$$

where T_a is the screen-level air temperature in Kelvin (K), σ the Stephan-Boltzmann's constant ($\sigma = 5.67 \times 10^{-8}$ W m^{-2} K^{-4}) and ε the clear-sky apparent emissivity. The clear-sky emissivity has been defined by many authors. We retain two definitions where ε is expressed either as a function of water vapor density, using water vapor pressure (noted e in hPa) and air temperature at the surface (noted T_a in Kelvin) [e.g., *Brutsaert*, 1975], or as a function of the column integrated water vapor (IWV in cm of precipitable water) [e.g., *Prata*, 1996]. The formulations of B75 (equation (2a)) and P96 (equation (2b)) are given as:

$$\varepsilon = A \times \left(\frac{e}{T_a}\right)^B \tag{2a}$$

$$\varepsilon = 1 - (1 + IWV) \times \exp\left(-(C + D \times IWV)^E\right) \tag{2b}$$

[11] In the B75 formulation (equation (2a)), the effective atmospheric emissivity is proportional to e/T_a, that itself is proportional to the screen-level water vapor density. In the P96 formulation, the effective clear-sky emissivity is related to the column integrated water vapor (IWV),. A, B, C, D and E are parametric coefficients that can be fitted using a set of clear-sky data as described in section 2.2. In equation (1), it is assumed that the screen-level temperature is a good proxy for the effective radiative temperature of the clear atmosphere. The effectiveness of T_a will be affected by the deviation of the vertical profile of temperature (strong or weak negative lapse rates or even temperature inversions) with respect to an adiabatic vertical profile. In equations (2a) and (2b), it is assumed that either the screen-level density or the column integrated density of water vapor are adequate proxies for the effective emissivity of the atmosphere. Again the effectiveness of these proxies will depend the deviation of the vertical profile of water vapor density with respect to an adiabatic profile. Hence in the remainder of the paper, we will focus on vertical profiles of humidity and temperature.

3. Evaluation of Clear-Sky Emissivity Models

3.1. Calibration of B75 and P96 Models

[12] The clear-sky observation data set is first used to optimize the coefficients of the B75 and P96 parameterizations. The two parameterizations are compared to measured clear-sky longwave irradiances ($LW_{measured}$), considered as reference values. The best parametric coefficients are obtained by least squares method to minimize standard deviation and mean error.

[13] Table 2 shows the original B75 and P96 coefficients found in the literature. With original coefficients we obtain biases between modeled and observed longwave irradiances in excess of 10 W m^{-2} and standard deviations at about 15 W m^{-2}. This bias is due to geographic effects and/or measurement offset caused by instrument calibration and is likely to depend on mean local atmospheric conditions. Table 2 also shows the coefficients of the B75 and P96 parameterizations that best fit the clear-sky measurements. Three sets of coefficients are derived: (1) daytime only, (2) nighttime only and (3) day and night together. The optimized coefficients yield near zero biases, as expected, and reduce the standard deviation significantly. Daytime and nighttime performances are not consistent. This is particularly evident for the P96 parameterization

Table 2. Optimization of B75 and P96's Parameterizations[a]

	Coefficients				
B75 Model	A	B	Bias	σ	RMS
Brutsaert [1975]		1/7	−13.5	17.7	22.3
Optimized	1.24				
Day	1.194		0.1	7.9	7.9
Night	1.208		0.1	11.2	11.2
All	1.20		−0.1	9.8	9.8
	Coefficients				
P96 **Model**	**C**	**D**	**E**	**Bias**	σ	**RMS**
Prata [1996]	1.2	3.0	0.5	−11.5	13.4	17.6
Optimized						
Day	0.99	2.8		0.1	5.3	5.3
Night	1.21			−0.1	11.5	11.5
All	1.1			0.1	9.3	9.4

[a]Shown are coefficients, mean error (bias in W m^{-2}), standard deviation (σ in W m^{-2}) and root-mean-square (RMS in W m^{-2}).

where the standard deviation around the mean error is twice as large at night than during daytime. It reveals that the control parameters of the B75 and P96 equations are best suited to represent daytime processes. At night, the vertical temperature gradient near the surface varies greatly between sunset and sunrise. The formulations of equation (2) will typically underestimate the downwelling longwave flux when a temperature inversion occurs (often the case in clear-sky situations), as evidenced by the greater A and C coefficients obtained by fitting on nighttime only data.

3.2. Parametric Model Comparisons

[14] Next we compare residuals errors produced by each parameterization with respect to measured longwave irradiances ($LW_{measured}$). We define ΔLW_{B75} as ($LW_{B75} - LW_{measured}$) and ΔLW_{P96} as ($LW_{P96} - LW_{measured}$). Figure 1 shows two scatterplots: one showing $LW_{B75} - LW_{P96}$ versus ΔLW_{B75} and one $LW_{B75} - LW_{P96}$ versus ΔLW_{P96}. We find that when the B75 parameterization simulates well the measured irradiance (i.e., $|\Delta LW_{B75}| < 5$ W m^{-2}), the P96 parameterization also yields good results ($|\Delta LW_{P96}| < 5$ W m^{-2}). In this case the two equations produce results that are consistent with each other and consistent with the measurements (data shown in the two gray squares on Figure 1). Data outside the two gray squares represent situations where B75 and P96 equations yield estimates of the longwave irradiance inconsistent with each other and inconsistent with the measurements. So, Figure 1 reveals that the discrepancy between B75 and P96 simu-

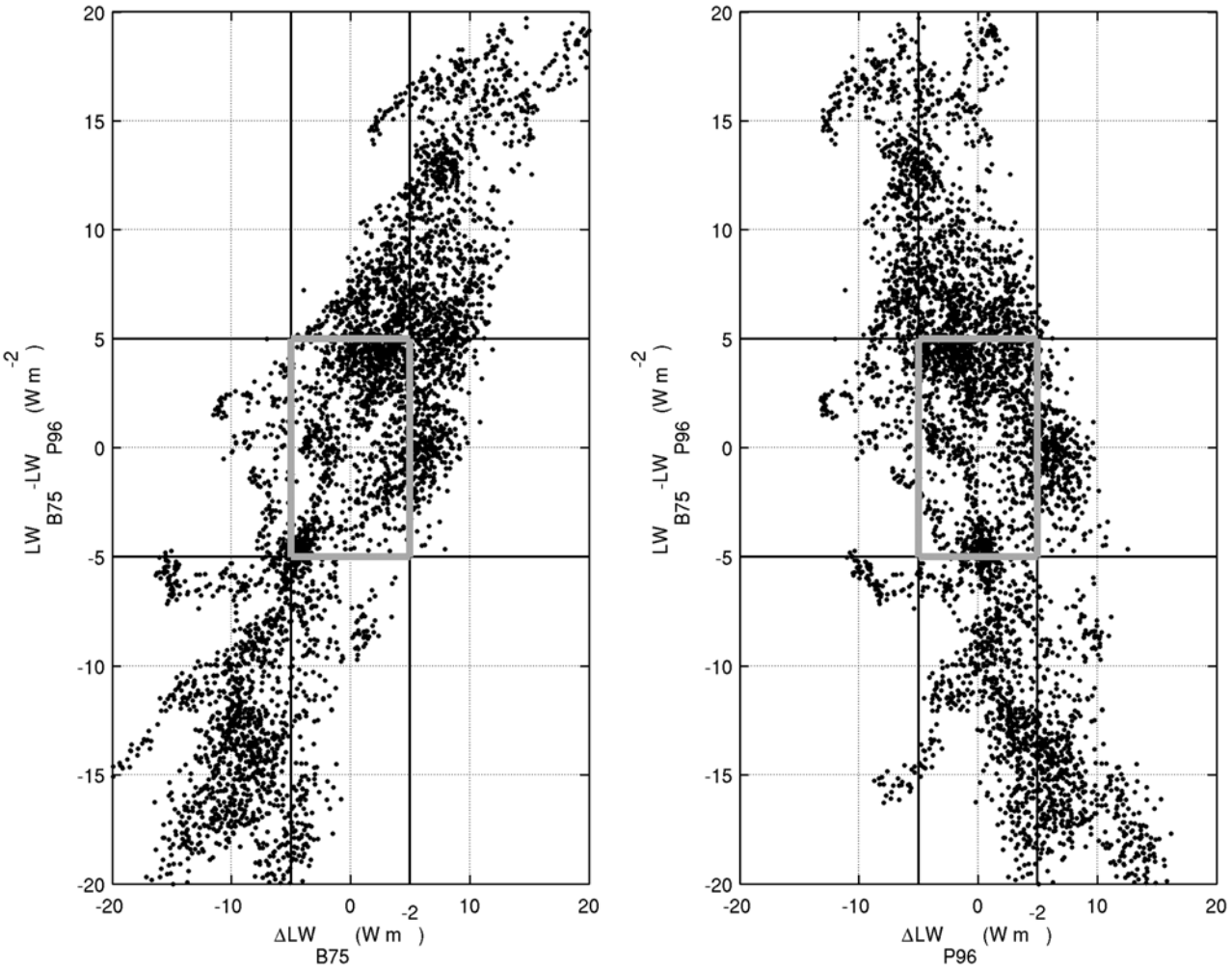

Figure 1. $LW_{B75} - LW_{P96}$ versus ΔLW_{B75} and $LW_{B75} - LW_{P96}$ versus ΔLW_{P96} (W m^{-2}) during daytime clear-sky conditions.

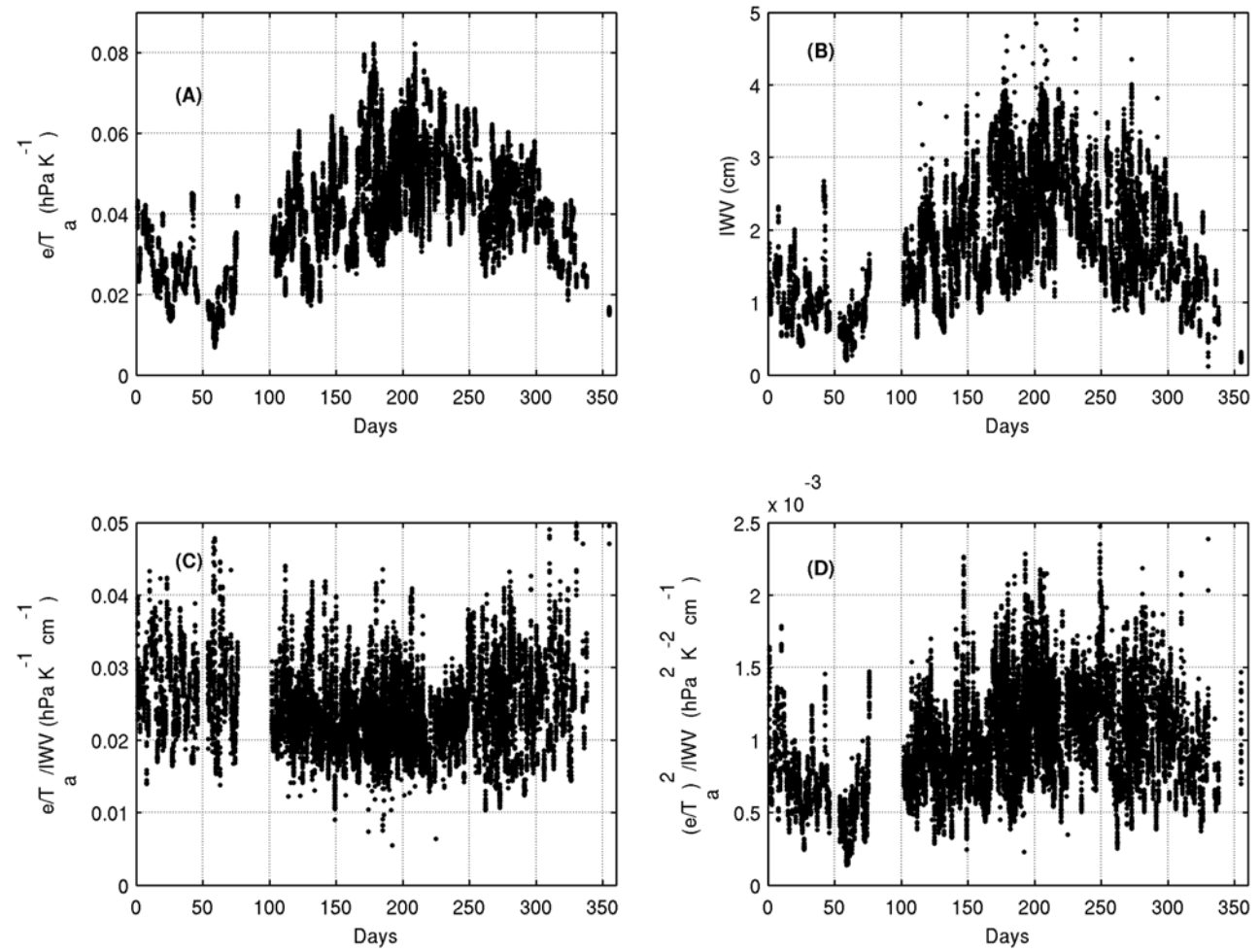

Figure 2. Time series e/T_a, IWV, (e/T_a)/IWV and $(e/T_a)^2$/IWV between May 2004 and October 2005.

lations could be used as a proxy to estimate B75 and P96 uncertainties relative to measurements. Hence in was follows, we study the difference between the B75 and P96 estimates to derive an improved estimate of the longwave irradiance. Given the formulations of B75 and P96 models (equation (2a)), we can hypothesize that the B75 and P96 discrepancies originate from relative variations of screen-level and column integrated water vapor density.

3.3. Emissivity Control Parameter

[15] Figure 2 shows time series e/T_a (A), IWV (B), (e/T_a)/IWV (C) and $(e/T_a)^2$/IWV (D). Terms e/T_a and IWV have pronounced variations at the annual timescale with a minimum in winter and a maximum during summer. Significant variations at the diurnal and synoptic scales are superimposed on the annual cycle. The (e/T_a)/IWV represents the relative weight of screen-level to column integrated water vapor density; it is a proxy for the effect of vertical distribution of water vapor on emissivity. (e/T_a)/IWV does not exhibit a strong annual cycle although values in summertime are somewhat smaller than in wintertime. Most of its variations are on short timescales (daily and synoptic). The sensitivity of clear-sky emissivity to water vapor vertical distributions is dominated by near surface variations. Additionally, this sensitivity is scaled by the near-surface water vapor density. When near-surface water vapor density is large, variations of upper layer water vapor density will have little impact. Hence, we find $(e/T_a)^2$/IWV to be an even more effective proxy for the effect of vertical distribution of water vapor on emissivity. $(e/T_a)^2$/IWV exhibits pronounced variations at all timescales (daily, synoptic and annual). It varies between 0.0001 $hPa^2\ K^{-2}\ cm^{-1}$ (in winter) and 0.0025 $hPa^2\ K^{-2}\ cm^{-1}$ (in summer). To quantify the impact vertical distribution of humidity on clear-sky emissivity, we use the Santa Barbara Disort Atmospheric Radiative Transfer (SBDART) code [*Ricchiazzi et al.*, 1998]. SBDART is used here to perform water vapor sensitivity tests on longwave emissivity in clear-sky conditions and also to quantify the impact of input parameters of the B75 and P96 parameterizations. This test consists in keeping the screen-level water vapor density constant while varying IWV (i.e., translation of humidity vertical profile in upper layers of atmosphere) to move the relative weight of water vapor density up and down in the atmospheric column. We use standard Mid Latitude Winter (MLW) and Mid Latitude Summer (MLS) vertical profiles of temperature, humidity and ozone. IWV is 0.854 cm (MLW) and 2.924 cm (MLS). Screen-level water vapor density is 3.5 g m^{-3} (MLW) and 14.0 g m^{-3} (MLS). For comparison, at the SIRTA obser-

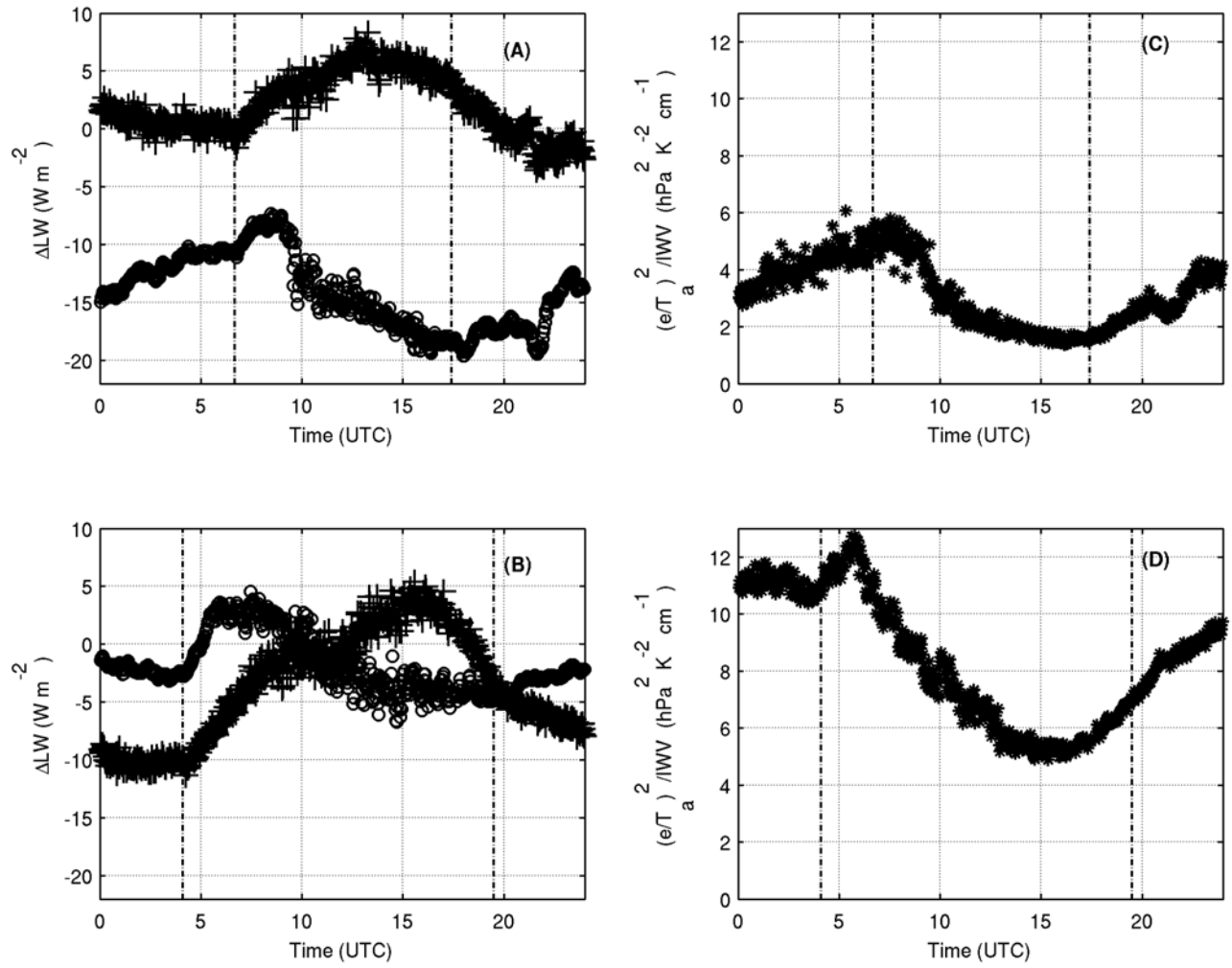

Figure 3. (a and b) Daily variations of longwave irradiance differences (ΔLW_{B75} indicated by circle and ΔLW_{P96} indicated by plus) and (c and d) ratio $(e/T_a)^2$/IWV for two clear-sky days. Figures 3a and 3c correspond to 28 February 2005, and Figures 3b and 3d correspond to 24 May 2004. Vertical dashed lines correspond to sunrise and sunset.

vatory, IWV varies from 0.2 cm to 4.1 cm between winter and summer. SBDART simulations allow us to reach a relationship between clear-sky emissivity and proxies of vertical distribution of humidity, namely (e/T_a)/IWV and $(e/T_a)^2$/IWV.

[16] We find the sensitivity of clear-sky emissivity to (e/T_a)/IWV to be approximately twice as important for MLS than for MLW (slope near 2.5 hPa^{-1} K cm and 5.3 hPa^{-1} K cm, respectively). Similarly we find the sensitivity of emissivity to $(e/T_a)^2$/IWV to be 145 hPa^{-2} K^2 cm and 82 hPa^{-2} K^2 cm for MLW and MLS, respectively. This reveals that (e/T_a)/IWV is not an adequate proxy as it implies that the emissivity will be more sensitive to the vertical distribution of water vapor in summertime than in wintertime. Conversely, $(e/T_a)^2$/IWV produces twice as much sensitivity in wintertime than in summertime. This is consistent with the fact that the moist (in terms of absolute humidity) surface layer in summertime will mask more efficiently the upper layers than in case of dry surface layers (winter).

[17] Next, we select two clear-sky periods lasting 24 h in winter and spring to analyze ΔLW_{B75}, ΔLW_{P96} and $(e/T_a)^2$/IWV variations. Figure 3 shows that discrepancies of the two models evolve during the day, in close relation with $(e/T_a)^2$/IWV. On 28 February 2005, ΔLW_{B75} displays a significant negative bias. Indeed, the surface layer is very dry compared to the rest of the atmosphere thus inducing a low clear-sky emissivity in the B75 equation. On the other hand, the P96 model agrees better with measurements with a maximum difference of 8 W m^{-2} due to a very dry surface layer. The surface layer is much more wet on 24 May 2004 (average $(e/T_a)^2$/IWV of 9×10^{-4} hPa^2 K^{-2} cm^{-1}) compared to 28 February 2005 (average $(e/T_a)^2$/IWV of 3×10^{-4} hPa^2 K^{-2} cm^{-1}) and consequently the B75 model agrees better with measurements (maximum difference of -8.5 W m^{-2}).

4. Improvement of Parametric Models

4.1. Optimization Based on the Vertical Profile of Humidity

[18] Clear-sky emissivity calculated with P96 (equation (2b)) depends only on IWV. However, SBDART simulations

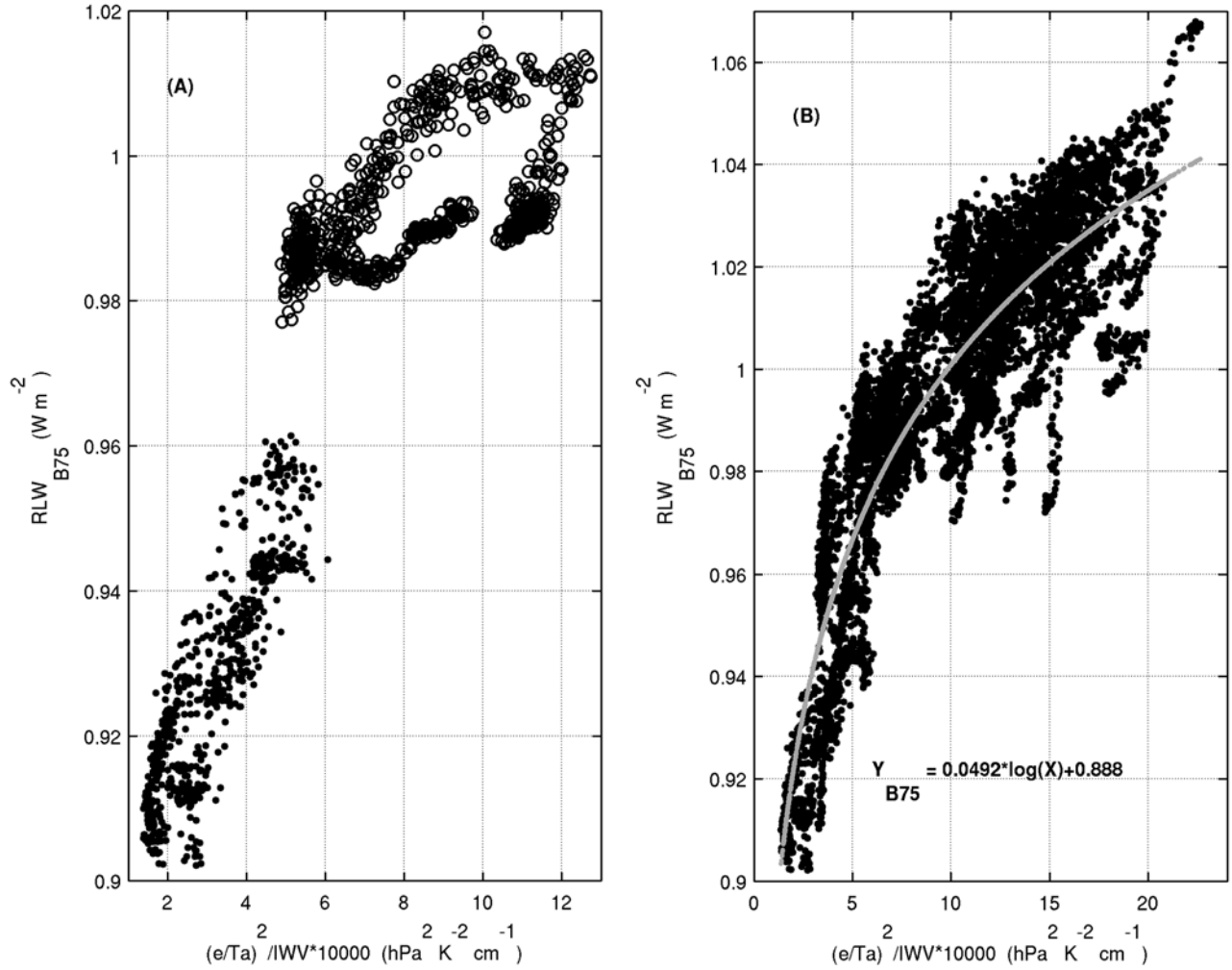

Figure 4. RLW_{B75} versus $(e/T_a)^2$/IWV (a) for two clear-sky days and (b) for all clear-sky days between May 2004 and October 2005. In Figure 4a, dots correspond to 28 February 2005, and circles correspond to 24 May 2004. In Figure 4b, gray curve represents the best logarithmic fit optimized by the least squares method.

described in section 3.3 shows that for a constant IWV, the clear-sky apparent emissivity is sensitive to the vertical distribution of humidity. In Figure 4, we show the ratio of calculated (B75) to measured clear-sky longwave irradiance, noted RLW_{B75}, as a function of the vertical distribution of water vapor $(e/T_a)^2$/IWV for all clear-sky situations. Figure 4a shows a scatterplot for two separate days, while Figure 4b shows a scatterplot based on 16 clear-sky days. Figure 4 shows that RLW_{B75} is close to 1.0 for a given value of $(e/T_a)^2$/IWV (near 12×10^{-4} hPa^2 K^{-2} cm^{-1}) that corresponds to an atmosphere where the vertical distribution of humidity is such that e/T_a is the correct proxy to estimate the clear-sky emissivity. When $(e/T_a)^2/IWV < 12 \times 10^{-4}$ hPa^2 K^{-2} cm^{-1} the vertical distribution of humidity is weighted higher in the atmosphere, hence the B75 equation will underestimate the longwave irradiance. When $(e/T_a)^2/IWV > 12 \times 10^{-4}$ hPa^2 K^{-2} cm^{-1} humidity is more concentrated near the ground than in the average profile and hence the B75 equation overestimates the longwave irradiance. Figure 4a reveals significant day-to-day and intradiurnal variations of $(e/T_a)^2$/IWV. A log fit is derived from the data on Figure 4b. The relationship between the RLW_{B75} term and $(e/T_a)^2$/IWV is not linear. Hence the atmospheric effective emissivity is more sensitive to the vertical distribution of water vapor when the surface layer is dry compared to the whole column. When the surface layer is humid, the shape of vertical profile above the humid layer has a smaller impact on the longwave irradiance.

[19] We derive a new empirical parameterization to estimate the downwelling irradiance from ground-based measurements of screen-level temperature and humidity and integrated water vapor content:

$$LW_{01} = \underbrace{\left[\frac{1.20 \times (e/T_a)^{1/7}}{\underbrace{\alpha \times \log\left(\frac{(e/T_a)^2}{IWV} \times 10^4\right) + \beta}_{Y_{B75}}}\right]}_{\varepsilon_{01}} \sigma \times T_a^4 \qquad (3)$$

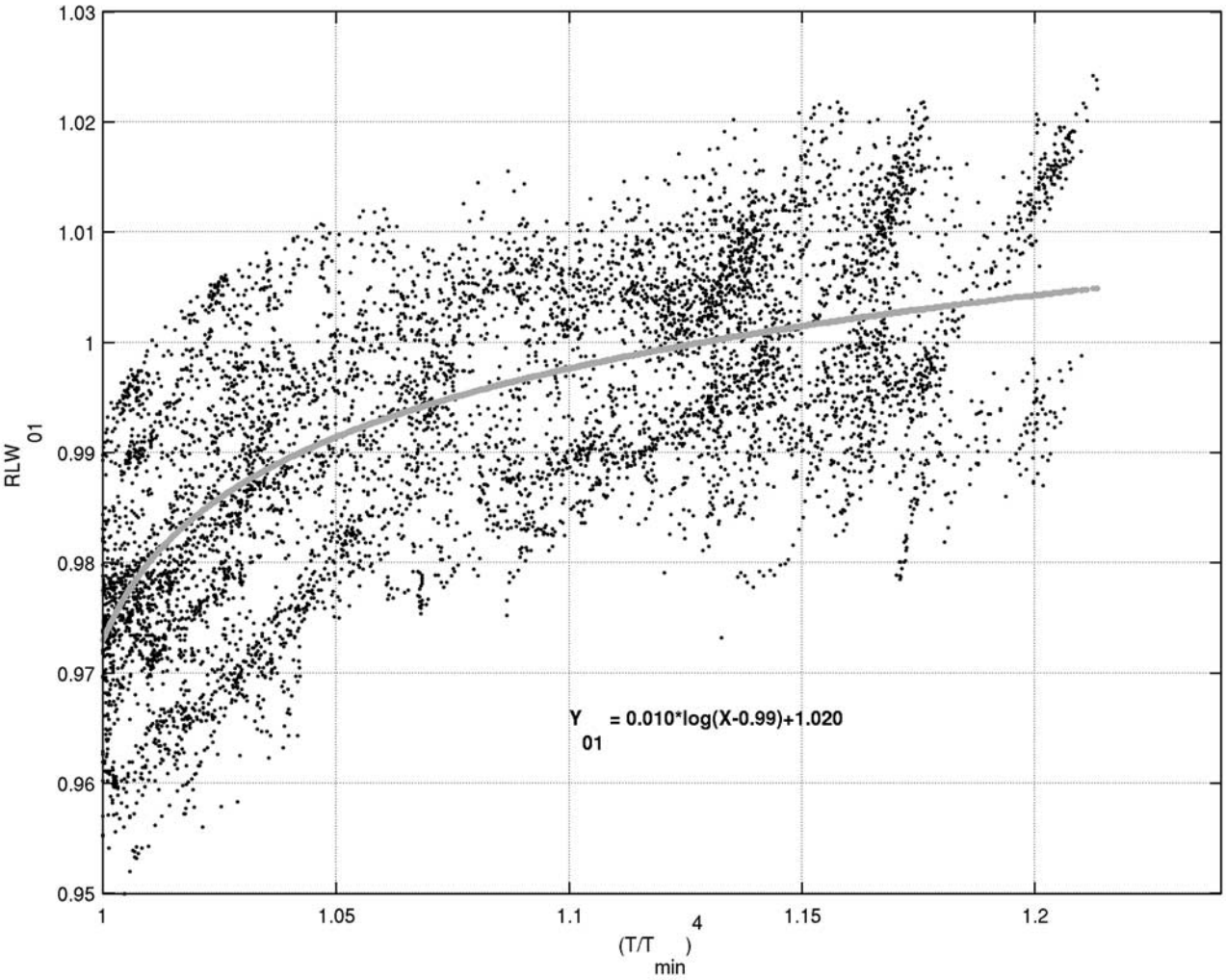

Figure 5. Scatterplot of RLW_{01} versus the $(T_a/T_{min})^4$ for all clear-sky periods and best logarithmic fit noted Y_1 optimized by the least squares method.

where α and β are fitted coefficients adjusted by the least squares method ($\alpha = 0.0492$ and $\beta = 0.888$).

[20] This relationship includes the impact of vertical distribution of humidity to improve the performance of the B75 model. Vertical distribution of humidity allows us to decrease significantly the discrepancies of B75 (discussed in section 4.3) for both daytime and nighttime periods. We also note $\Delta LW_{01} = LW_{01} - LW_{measured}$ and residual errors are analyzed in section 4.2.

4.2. Optimization Based on Diurnal Cycle of Surface Temperature

[21] In most cases, discrepancies between B75 and/or P96 estimates and measurements, ΔLW_{B75} and ΔLW_{P96} respectively, are not constant with the time of the day. We showed in the previous section that variations in the vertical distribution of humidity can explain an important part of these discrepancies (see section 4.3). The accuracy of the B75 and P96 models are also affected by the rate of heating and cooling of the surface with respect to that of the radiatively significant atmospheric layer above the surface. During daytime, solar radiation heats the surface faster than the atmosphere above; as a result the screen-level T_a will overestimate the effective radiative temperature. This leads to an overestimation of the computed downwelling longwave irradiance. During a clear-sky night, the high-emissivity surface cools faster than the atmosphere above it reducing the temperature lapse rate or even creating a surface layer inversion, leading to an underestimation of the computed longwave irradiance. Hence during cooling and heating portions of the day, the vertical profile of temperature near the ground may vary significantly.

[22] To take into account the impact of the vertical profile of temperature, we consider an additional control parameter, defined as the ratio $(T_a/T_{min})^4$. In this expression, T_a is the screen-level temperature measured at two meters height, and T_{min} is the minimum temperature during the day. T_a and T_{min} are expressed in Kelvin. This term accounts for the daytime and nighttime cycles of the screen-level temperature and is here considered as a proxy for the temperature lapse rate. It is analogous to the sinusoidal function used by *Dürr and Philipona* [2004] to represent diurnal cycle of temperature lapse rate. The term RLW_{01} is defined as the ratio of LW_{01} (from equation (3)) to $LW_{measured}$. Figure 5 displays the scatter-

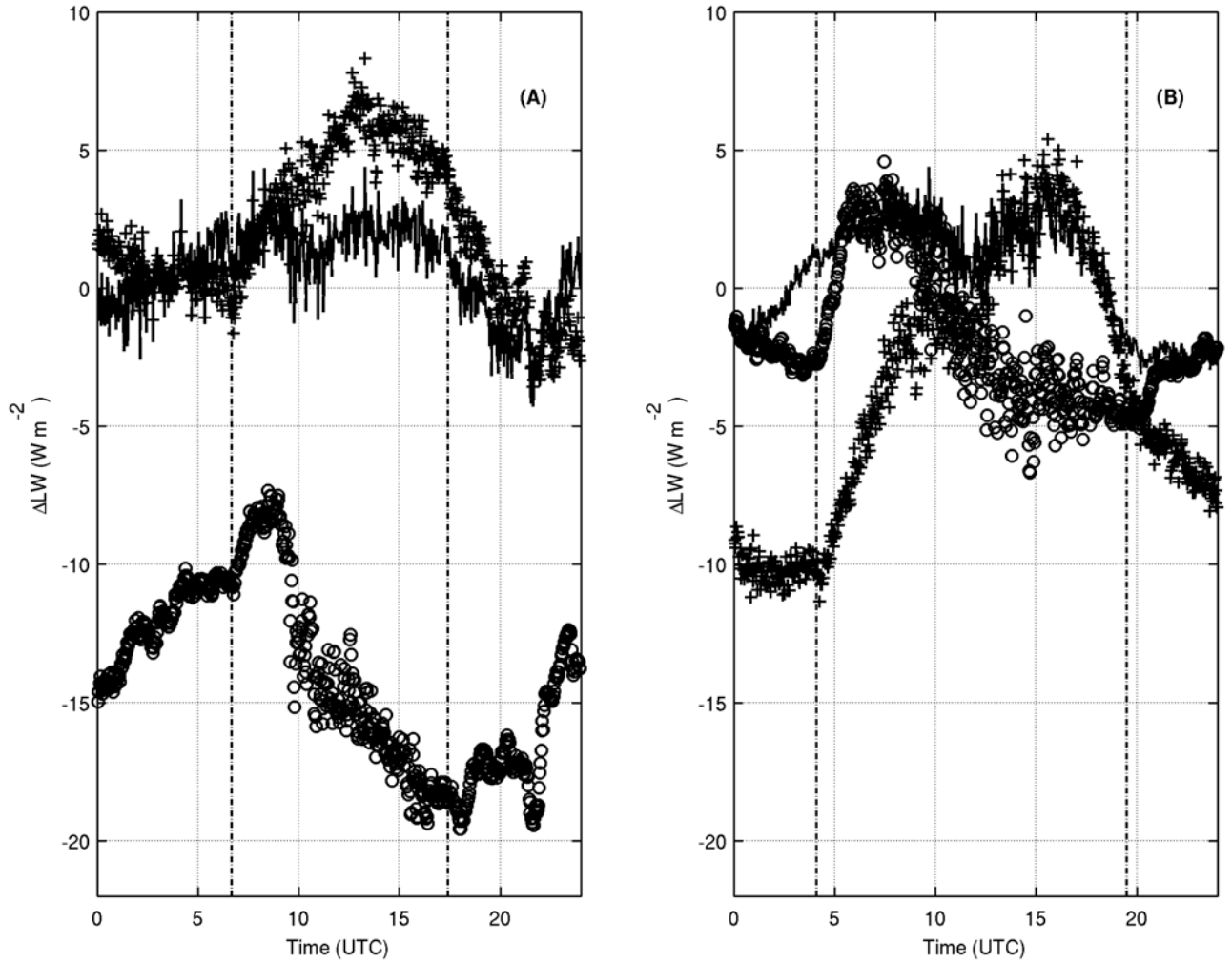

Figure 6. ΔLW versus time computed on (a) 28 February 2005 and (b) 24 May 2004. Circles correspond to irradiance difference with B75's model (equation (2a)). Pluses represent irradiance difference with P96's model (equation (2b)). Line corresponds to irradiance difference with the optimized model (equation (4)). Vertical dashed lines correspond to sunrise and sunset.

plot of RLW_{01} as a function $(T_a/T_{min})^4$. The polynomial fit Y_{01} shown in Figure 5 is derived to correct the effective radiative temperature of equation (1). Figure 5 shows that Y_{01} is close to 1.0 for a given value of $(T_a/T_{min})^4$ (near 1.1). This corresponds to an atmosphere where the vertical profile of temperature is well taken into account by the LW_{01} model (equation (3)). When $(T_a/T_{min})^4 < 1.1$, Y_{01} is smaller than unity leading to an increased radiative temperature and an increased LW_{01} irradiance. These periods correspond typically to nighttime periods characterized by a small lapse rate of temperature, where T_a underestimates the effective radiative temperature. When $(T_a/T_{min})^4 > 1.1$, Y_{01} is greater unity leading to a decrease of the overestimated temperature. The term $(T/T_{min})^4$ is able to explain a significant part of the B75 and P96 model uncertainties (discussed in section 4.3) for both daytime and nighttime periods.

[23] The final expression of the new model considers two control parameters based on vertical distribution of humidity and diurnal cycle of temperature. It is defined as:

$$LW_{02} = \underbrace{\left[\frac{1.20 \times \left(e/T_a\right)^{1/7}}{\alpha \times \log\left(\frac{(e/T_a)^2}{IWV} \times 10^4\right) + \beta}\right]}_{\varepsilon_{01}} \times \sigma \times \left[\frac{T_a}{\left[\underbrace{\gamma \times \log\left((T_a/T_{min})^4 - 0.99\right) + \delta}_{Y_{02}}\right]^{1/4}}\right]^4 \quad (4)$$

where $\alpha = 0.0492$, $\beta = 0.888$, $\gamma = 0.010$ and $\delta = 1.020$.

Table 3. Statistical Scores of the B75, P96, and Optimized Clear-Sky Longwave Parameterizations Given by Equations (3) and (4)[a]

Periods	Models	Bias	σ	RMS
All	B75	−0.1	9.8	9.8
All	P96	0.1	9.3	9.3
All	equation (3)	−0.9	4.7	**4.7**
All	equation (4)	0	3.8	**3.8**
Daytime	B75	0.1	7.9	7.9
Daytime	P96	0.1	5.3	5.3
Daytime	equation (3)	1.0	3.7	**3.8**
Daytime	equation (4)	0.8	3.2	**3.3**
Nighttime	B75	0.1	11.2	11.2
Nighttime	P96	−0.1	11.5	11.5
Nighttime	equation (3)	−2.1	5.2	**5.6**
Nighttime	equation (4)	−0.8	4.2	**4.3**

[a]Unit is W m^{-2}. Bold values correspond to results obtained by the new model developed in this study.

4.3. Evaluation of the New Model

[24] To evaluate the accuracy of this optimized model, we use the term $\Delta LW_{02} = LW_{02} - LW_{measured}$ which permits us to quantify the accuracy of the new model (equation (4)). Figure 6 shows examples of model errors (ΔLW_{B75}, ΔLW_{P96} and ΔLW_{02}) for a winter and a summer situation, for the B75 (equation (2a)), P96 (equation (2b)) and new (equation (4)) models. The B75 and P96 models use the optimized coefficients defined in Table 2. Figure 6 shows that the ΔLW_{02} error is considerably reduced with the new model both during daytime and nighttime.

[25] Next we apply the model to the selected 16 clear-sky days and clear-sky nights in the May 2004 to October 2005 data set. Table 3 shows the performances of ΔLW_{B75}, ΔLW_{P96}, ΔLW_{01} and ΔLW_{02} for all, daytime and nighttime periods. For ΔLW_{B75} and ΔLW_{P96}, we apply the best parametric coefficients adjusted by the least squares method (Table 2) that yields near zero biases. For ΔLW_{01}, RMS errors are reduced by a factor 1.7 for daytime periods and a factor 2 for nighttime periods. The bias is −0.9 W m^{-2} on average. It is +1.0 W m^{-2} for daytime periods and −2.1 W m^{-2} for nighttime periods. For ΔLW_{02}, RMS errors and standard deviations are reduced by a factor 2 for daytime periods and a factor 2.7 for nighttime periods. The LW_{02} model is unbiased on average. The bias is +0.8 W m^{-2} and −0.8 W m^{-2} for daytime and nighttime periods, respectively.

[26] To validate the new model with an independent sub data set of the SIRTA database, we use all clear-sky daytime 15-min periods outside the long clear-sky events exceeding 6 h. We use 415 periods of 15 min between May 2004 and October 2005 that are different from the time periods used to optimize the new algorithm. Table 4 shows the improvement brought by the two optimized parameterizations (equations (3) and (4)). All the RMS errors are globally less important for this sub data set compared to Table 3. However, both B75 and P96 models have a more important bias than previously of +1.7 W m^{-2} and −0.6 W m^{-2}, respectively. This is due to the fact that the parametric coefficients were optimized on the data set with clear-sky event exceeding 6 h. ΔLW_{02} remains unbiased however. The absolute maximum discrepancies are less than 10 W m^{-2} and the RMS errors less than 3 W m^{-2}. Note that accounting for the proxy $(T/T_{min})^4$ in LW_{02} model allows us to remove the small bias (−0.3 W m^{-2}) associated with the LW_{01} model.

5. Conclusion

[27] The most common control parameters found in the literature to simulate the clear-sky surface downwelling longwave irradiance are screen-level temperature, screen-level water vapor density, and column integrated precipitable water. Over a dozen studies derived new or optimized empirical relationships that relate these control parameters to the longwave irradiance. *Brutsaert* [1975] established that screen-level water vapor density is an efficient proxy to estimate the effective emissivity of the cloud-free sky. *Prata* [1996] establishes that the integral of the water vapor density profile is an event more efficient proxy to estimate the effective clear-sky emissivity. Like many authors before us, we derive local parametric coefficients in order to optimize the performance of both B75, and P96. When we focus on nighttime periods, B75 and P96 optimized with nighttime specific parameters have similar performances (11 W m^{-2} RMS error) when compared to actual measurements. When optimized coefficients are derived on the basis of daytime measurements only, the RMS uncertainty of B75 is about 8 W m^{-2}, while that of P96 is about 30% less. Finally when both day and night periods are simulated with the same coefficients, both B75 and P96 simulate the clear-sky longwave irradiance with an uncertainty of about 10 W m^{-2} RMS error.

[28] Using the SBDART radiative transfer code we make a sensitivity test to quantify the impact of the ratio of screen-level to column-integrated water vapor density $(e/T_a)^2/IWV$ on clear-sky effective emissivity in winter conditions. This test reveals that variations in vertical distribution of water vapor can induce variations in clear-sky effective emissivity as large as 25%. Similarly, variations of the temperature lapse rate can explain about 4% of the variability of downwelling longwave irradiance (winter conditions). Next we demonstrate that 49% of the uncertainty in B75 simulations can be explained by the term $(e/T_a)^2/IWV$ (section 4.1). We propose a new formulation (equation (3)) where the clear-sky emissivity accounts for both the screen-level water vapor density and the $(e/T_a)^2/IWV$. Another 12% of B75 uncertainty can be explained by the variations in the shape of the vertical temperature profile compared to an average one. This is particularly evident after sunrise when the rate of heating of the surface is faster than that of the layer of atmosphere above, or during clear-sky nights when a shallow surface inversion appears after sunset. We simulate this change of temperature lapse rate using the diurnal range of temperature. The final formulation (equation (4)) allows us

Table 4. Downwelling Longwave Flux Errors for Selected Diurnal Periods of 15 Min[a]

Models	Bias	σ	RMS
B75	1.7	6.2	6.3
P96	−0.6	4.6	4.7
Equation (3)	−0.3	3.3	**3.4**
Equation (4)	0.1	2.7	**2.7**

[a]Unit is W m^{-2}. Bold values correspond to results obtained by the new model developed in this study.

to simulate the downwelling longwave irradiance during daytime and nighttime periods with an RMS uncertainty less than 5 W m^{-2}. Such a parameterization opens up new possibilities to study the effect of high-altitude clouds on the longwave irradiance at the surface, that until now contributed at the uncertainty level. This will enable us to quantify their importance on the energy balance at the ground.

[29] **Acknowledgments.** We would like to acknowledge the Association Nationale de Recherche Technique (ANRT) and the company ATMOS for their financial support throughout this study.

References

Ångström, A. (1918), A study of the radiation of the atmosphere, *Smithsonian Misc. Collect.*, *65*, 1–159.

Bernstein, L., and the Core Writing Team (2007), *Climate Change 2007: Synthesis Report, Intergovernmental Panel on Climate Change Fourth Assessment Report*, Cambridge Univ. Press, New York.

Bock, O., and E. Doerflinger (2001), Atmospheric modeling in GPS data analysis for high accuracy positioning, *Phys. Chem. Earth*, *26*, 373–383.

Bony, S., J.-L. Dufresne, H. Le Treut, J.-J. Morcrette, and C. Senior (2004), On dynamic and thermodynamic components of cloud change, *Clim. Dyn.*, *22*(2–3), 71–86, doi:10.1007/s00382-003-0369-6.

Brunt, D. (1932), Notes on radiation in the atmosphere, *Q. J. R. Meteorol. Soc.*, *58*, 389–420.

Brutsaert, W. (1975), On a derivable formula for long-wave radiation from clear skies, *Water Resour. Res.*, *11*, 742–744.

Cess, R., et al. (1990), Intercomparison and interpretation of climate feedback processes in 19 atmospheric general circulation models, *J. Geophys. Res.*, *95*, 16,601–16,615.

Chen, T., W. B. Rossow, and Y. Zhang (2000), Radiative effects of cloud-type variations, *J. Clim.*, *13*, 264–286.

Dong, X., B. Xi, and P. Minnis (2005), A climatology of midlatitude clouds from the ARM SGP central facility. Part II: Cloud fraction and surface radiative forcing, *J. Clim.*, *19*, 1765–1783.

Duarte, H. F., N. L. Dias, and S. R. Maggiotto (2006), Assessing daytime downward longwave radiation estimates for clear and cloudy skies in southern Brazil, *Agric. For. Meteorol.*, *139*, 171–181.

Dürr, B., and R. Philipona (2004), Automatic cloud amount detection by surface longwave downward radiation measurements, *J. Geophys. Res.*, *109*, D05201, doi:10.1029/2003JD004182.

Haeffelin, M., et al. (2005), SIRTA, a ground-based atmospheric observatory for cloud and aerosol research, *Ann. Geophys.*, *23*, 262–275.

Idso, S. B., and R. D. Jackson (1969), Thermal radiation from the atmosphere, *J. Geophys. Res.*, *74*, 5397–5403.

Illingworth, A. J., et al. (2007), CLOUDNET—Continuous evaluation of cloud profiles in seven operational models using ground-based observations, *Bull. Am. Meteorol. Soc.*, *88*, 883–898.

Kneizys, F. X., E. P. Shettle, L. W. Abreu, J. H. Chetwynd, G. P. Anderson, W. O. Gallery, J. E. A. Selby, and S. A. Clough (1988), Users Guide to LOWTRAN7, *Environ. Res. Pap., 1010 FGL-TR-88-0177*, Air Force Geophys. Lab., Hanscom Air Force Base, Mass.

Long, C. N., and T. P. Ackerman (2000), Identification of clear skies from broadband pyranometer measurements and calculation of downwelling shortwave cloud effect, *J. Geophys. Res.*, *105*, 609–625.

Morille, Y., M. Haeffelin, P. Drobinski, and J. Pelon (2007), STRAT: An automated algorithm to retrieve the vertical structure of the atmosphere from single-channel lidar data, *J. Atmos. Oceanic Technol.*, *24*, 761–775.

Niemelä, S., P. Räisänen, and H. Savijärvi (2001), Comparison of surface radiative flux parameterizations part I: Longwave radiation, *Atmos. Res.*, *58*, 1–18.

Ohmura, A. (1981), *Climate and Energy Balance of the Arctic Tundra*, *Zuricher Geogr. Schr.*, *3*, 448 pp., Geogr. Inst., Zurich, Switzerland.

Ohmura, A., et al. (1998), Baseline Surface Radiation Network (BSRN/WCRP): New precision radiometry for climate research, *Bull. Am. Meteorol. Soc.*, *79*, 2115–2136.

Prata, A. J. (1996), A new long-wave formula estimating downward clear-sky radiation at the surface, *Q. J. R. Meteorol. Soc.*, *122*, 1127–1151.

Ricchiazzi, P., S. Yang, C. Gautier, and D. Sowle (1998), SBDART: A research and teaching software tool for plane-parallel radiative transfer in the Earth's atmosphere, *Bull. Am. Meteorol. Soc.*, *79*(10), 2101–2114.

Ruckstuhl, C., R. Philipona, J. Morland, and A. Ohmura (2007), Observed relationship between surface specific humidity, integrated water vapor, and longwave downward radiation at different altitudes, *J. Geophys. Res.*, *112*, D03302, doi:10.1029/2006JD007850.

Shupe, M. D., and J. M. Intrieri (2003), Cloud radiative forcing of the Arctic surface: The influence of cloud properties, surface albedo, and solar zenith angle, *J. Clim.*, *17*, 616–628.

Snell, H. E., G. P. Anderson, J. Wang, J.-L. Moncet, J. H. Chetwynd, and S. J. English (1995), Validation of FASE (FASCODE for the Environment) and MODTRAN3: Updates and comparisons with clear-sky measurements, *Proc. SPIE Int. Soc. Opt. Eng.*, *2578*, 194–204.

Swinbank, W. C. (1963), Long-wave radiation from clear skies, *Q. J. R. Meteorol. Soc.*, *89*, 339–348.

Van Meijgaard, E., and S. Crewell (2005), Comparison of model predicted liquid water path with ground-based measurements during CLIWA-NET, *Atmos. Res.*, *75*, 201–226.

Watson, R. T., and the Core Writing Team (2001), *Climate Change 2001: Synthesis Report, Intergovernmental Panel on Climate Change Third Assessment Report*, Cambridge Univ. Press, New York.

T. Besnard, ATMOS Sarl, 9 rue Lucien Chaserant, F-72650 Saint Saturnin, France.

P. Drobinski, Institut Pierre Simon Laplace, Service d'Aéronomie, Université Pierre et Marie Curie, F-75252 Paris, France.

J.-C. Dupont, Institut Pierre Simon Laplace, Laboratoire de Météorologie Dynamique, Ecole Polytechnique, F-91128 Palaiseau, France. (jean-charles.dupont@lmd.polytechnique.fr)

M. Haeffelin, Institut Pierre Simon Laplace, Ecole Polytechnique, F-91128 Palaiseau, France.